Research Article | Vol. 33, No. 12 / 16 Jun 2025 / Optics Express 24800
Optics EXPRESS

Single pass fs writing of photonics components in low-iron soda lime glass through selective pulse number control

FOROOGH JAFARI,[1,*] JEAN-SÉBASTIEN BOISVERT,[1] RAMAN KASHYAP,[1,2] AND SÉBASTIEN LORANGER[1]

[1]Department of Electrical Engineering, PolyGrames, École Polytechnique Montréal, 2900 Édouard-Montpetit, Montreal, QC, H3 T 1J4, Canada
[2]Department of Physics Engineering, École Polytechnique Montréal, 2900 Édouard-Montpetit, Montreal, QC, H3 T 1J4, Canada
*foroogh.jafari@polymtl.ca

Abstract: This article presents single-pass, ultra-fast laser writing of different photonic components, based on modulating the laser pulse picker by an arbitrary waveform. The effect of various writing parameters on the induced refractive index change for obtaining *positive* index single-mode waveguides inside a low-iron soda lime glass sample is studied. An index contrast of 5.8×10^{-3} is achieved. The technique can also inscribe a strong uniform Bragg grating waveguide (BGW) in the same writing passage with a transmission dip of 35 dB in the C-band, a mode taper to match a standard single-mode fiber, and a no-bend coupler. The inscription of BGW shows a strong dependence on the laser polarization state relative to the scan direction. Polarization parallel to the scan direction increases the attenuation level by around 10 dB compared to the orthogonal state writing. Furthermore, we show that the capability of this method for inscribing tapered waveguides improves coupling efficiency to the smf-28 fiber by an amount of 3.26 dB compared to the un-tapered waveguide. The effect of pulse numbers on mode-field diameter (MFD) allows the inscription of straight couplers with coupling constants ranging from 16.6 m^{-1} to 42.4 m^{-1} which has the benefit of no bending loss.

1. Introduction

Ultrafast laser micromachining in optically transparent materials has been studied extensively and gained interest both in science and for applications, e.g., enabling the 3D fabrication of photonic circuits. Compared to the technology of photolithography, ultrafast laser micromachining is not restricted to the substrate surface and it is mask-free providing more flexibility in circuit design and reducing the cost of prototyping. Inscription of photonics components with a fs laser inside transparent materials is a result of nonlinear effects that generate a free electron plasma. These excited electrons transfer their energy to the lattice, and lead to morphological changes in the material which are responsible for a permanent refractive index (RI) change [1]. Depending on the exposure parameters, the RI change can be either positive or negative relative to the background RI. Different types of waveguides are demonstrated in a variety of materials, including depressed index cladding waveguides [2], stress-field induced double-line waveguides [3] and positive-index single-line waveguides [4], based on the sign of the RI change. Boisvert et al. have recently shown that positive-index RI change can be obtained in a broader range of glasses than was previously believed, through increasing the laser fluence [5].

In this article, we demonstrate functional devices written in a single-pass using a positive RI change by fs exposure in low-iron soda lime glass. The functional devices demonstrated are Bragg-grating waveguides for selective reflection, tapered waveguides for mode-field adaptation

#562100 https://doi.org/10.1364/OE.562100
Journal © 2025 Received 12 Mar 2025; revised 15 May 2025; accepted 17 May 2025; published 3 Jun 2025

Optics EXPRESS

and no-bend couplers for power splitting. To achieve positive-index single-pass writing, the exposure parameters and pulse control are carefully optimized.

To create a Bragg grating waveguide (BGW), there are two possible writing methods: double-step inscription, where the waveguide and grating pattern are inscribed sequentially in two separate processes, or single-step inscription where both are inscribed in a single-pass process. The former [3,6] provides more control over the parameters as both waveguide and Bragg grating (BG) can be inscribed with different exposure conditions, at the cost of inscription time. Also, since material photosensitivity is depleted during waveguide inscription, second exposure might not lead to high RI modulation in BGW. In contrast, the single-step approach is much faster and can lead to strong BGs since the maximum contrast of RI change can be utilized. The downside of this approach is less control over the numerical aperture (NA) of the waveguide, thus the mode-field diameter (MFD), as the exposure and pulse conditions are constrained by the BG requirements as well. Uniform BGW [7,8], phase-shifted BGW [9], and apodized BGW [10] are examples of different kinds of gratings written using the single-step approach on fused silica and Borosilicate glasses. Depending on the energy of pulses involved in inscribing each voxel, it can lead to type I or type II gratings [11]. The latter generally appears for high pulse energy and is associated with higher losses. Therefore, to maintain low insertion loss and strong RI modulation, a burst of multiple low-energy pulses is required to form each voxel. Burst of pulses can be generated by an external acousto-optic modulator [7–10] or through control of an internal pulse picker integrated inside the fs laser system, which is the method of control used in this paper and has the advantage of no added external component.

Another useful laser-inscribed photonic devices are tapered waveguides, where the MFD is adiabatically changed to adapt an input device, e.g. an optical fiber, to an integrated platform [12]. Mode profile mismatch between inscribed photonic components and single-mode fiber is one of the main limitations in scaling up of integrated photonic circuits. In glasses, the tapered waveguide have been fabricated by linearly changing the pulse energy with an attenuator [13] or doing multiple reruns after the initial inscription with a lower power level [14]. Instead of changing the pulse energy that affects the nonlinear photoionization rate, we demonstrate tapers by simply changing the pulse numbers. By keeping the pulse energy constant but varying the pulse rate, which predominantly influences the heat affected zone, it is possible to separate the effect of linear and nonlinear contributions, making the RI change calibration more repeatable, rigorous and adaptable to varying experimental conditions. To do so, we first optimize the exposure parameters to obtain a waveguide with maximum mode confinement, and then apply a pulse activation control, to gradually change the waveguide NA. Deliberate control of pulse numbers can open a fast and feasible way of designing complex photonics structures such as couplers. As an example, we inscribed symmetric straight couplers with an advantage of no bending loss.

We systematically studied various control waveforms using an arbitrary waveform generator to fabricate not only high-reflectivity BGWs, but also tapered waveguides to adapt input mode-field diameter and two-port power splitter, all in a single step. The proposed method enables the direct inscription of multiple photonic components without requiring additional optical elements, such as an acousto-optic or spatial light modulator. This simplifies the fabrication process, reducing cost, and power limitations [15] while enhancing scalability and mass production capability. The key to this fabrication process is the control waveform as well as a positive index-change induced by fs inscription. While there is an extensive study on fs laser-induced RI modification in a wide variety of compound glasses [5,16,17], there remains a gap in the study of soda lime glass. Our finding reveals that at low net fluence without heat accumulation, RI change is negative. However, as net fluence increases, the RI change transitions from negative to positive. Further increasing the net fluence results in a nonuniform RI change, where the central region exhibits

Optics EXPRESS

a lower RI change, surrounded by higher positive side lobes. This imposes a constraint on the fluence range suitable for waveguide inscription.

2. Inscription method

A Pharos fs laser at a wavelength of 1030 nm with a pulse duration of 250 fs doubled to 515 nm with the Hiro system. The repetition rate of the laser was controlled by a pulse picker with the highest available value of 606 kHz. The maximum pulse energy of fs laser at 515 nm was 8.3 μJ. As shown in Fig. 1(a) the sample is translated along the x-axis with a constant velocity. The beam arrives transverse to the waveguide, which allows for custom writing shapes not limited in length. The beam is focused 100 μm below the top surface (z-axis) of a 75 mm long low-iron soda lime glass (Fisherbrand, Catalog No.: 12-550-A3, band gap energy ~ 4.5 eV) sample by a 40X plan achromat objective lens with an NA = 0.65. The linear Rayleigh focal spot is estimated to be 1 μm in transverse plane (x-y axis) and 1.3 μm in propagation direction (z-axis). The sample was placed on a high precision XYZ air-bearing Aerotech stage to be translated at a constant velocity. Writing complex structures in a single step requires having control on the number of fs laser pulses delivered on a sub-wavelength length scale. While modern lasers may offer pulse-on-demand feature, such features are not available ubiquitously and all lasers are not equal in their versatility and applicability. Therefore, we propose to externally control the pulse-picker, to ensure our demonstration remains independent of any specific laser. Figure 1(b)-(d) conceptually shows how this method can be utilized for writing first-order BGWs, high-order BGWs and tapered waveguides.

The TTL 2.5 V signal level opens the pulse picker, while a 0 V stops pulse emission. To create a BGW, it is required to create an additive RI modulation satisfying the Bragg condition expressed as:

$$\Lambda = \frac{m\lambda_B}{2n_{eff}} \tag{1}$$

where Λ is the grating period, λ_B is the Bragg wavelength, m is the grating order and n_{eff} is the effective RI of the propagating mode. Polarization of the fs laser is linear, and we control its direction relative to the scan direction by a half-wave plate. The results showing grating strength has strong dependency on the laser polarization direction which will be discussed later. Two methods of pulse modulation are studied: on-off keying (Fig. 1(b)) and frequency shift keying (FSK) (Fig. 1(c)).

The Bragg transmission loss dip is a measure of grating strength and is logarithmically proportional to the product of mode overlap integral with the RI change area and the RI change depth [18]. Hence it is important to select exposure conditions carefully to maintain the highest mode confinement, thus maximizing overlap, and larger index contrast between "low exposed" and "high exposed" voxels, simultaneously. In our setup, even by considering the nonlinear cross section, the focused spot size is < 1 μm, it is still larger than the grating period, and therefore there is an overlap between the voxels when writing in the 1st order as shown in Fig. 1(b). This limits the RI modulation depth, but said modulation is still sufficient to get strong gratings in the 1st order. Due to this limitation, simple on-off keying remains the more effective strategy for BGW inscription, as shown by our results.

However, inscribing higher order gratings or long period gratings (LPG) in which the period is evidently much larger than the spot size, on-off keying would bring a problem of waveguide mode confinement, guiding loss and scattering due to the large unwritten gaps between each pulse burst. In such cases, FSK pulse modulation, as shown in Fig. 1(c), would be more effective, as it would maintain a minimum exposed, thus guiding region.

To inscribe the tapered waveguide, the MFD and n_{eff} of the propagating mode must change gradually to ensure adiabaticity. This can be obtained by changing the number of pulses (duty cycle of On-off keying) continuously during the scanning of the sample (Fig. 1(d)). Such a slow

Optics EXPRESS

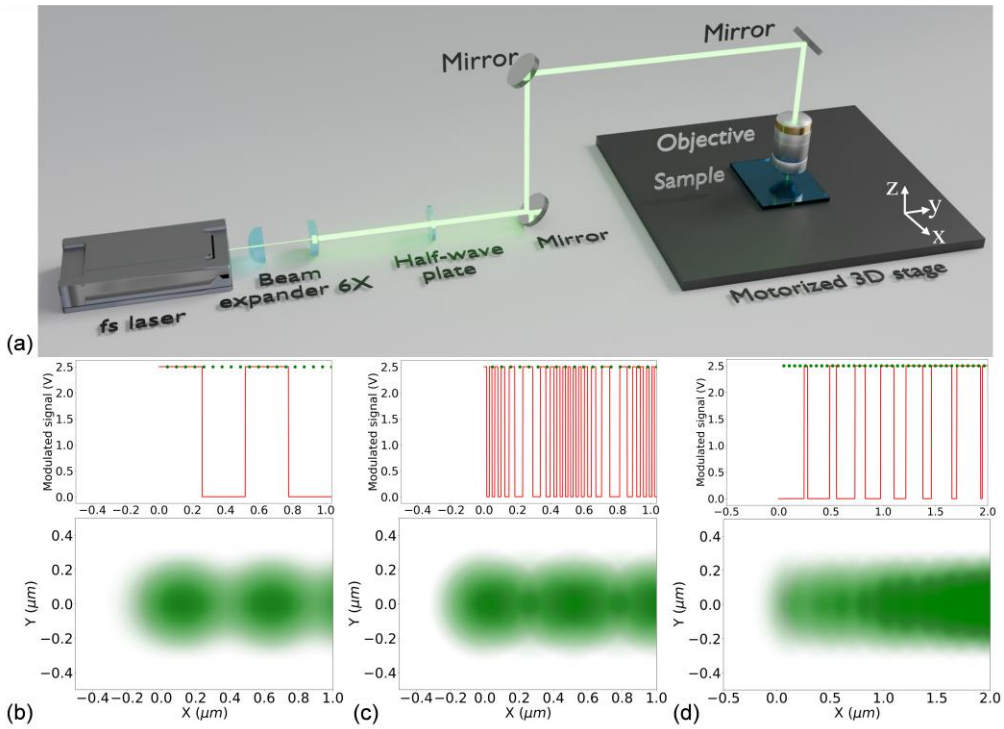

Fig. 1. (a) Schematic of the experimental setup for fs laser inscription on glass. A beam passes through a beam expander to match the numerical aperture of the objective. The half-wave plate is used for changing the polarization state of fs laser beam. The sample is held on an Aerotech 3D stage. (b) On-off keying and (c) FSK for BGW inscription and (d) variable duty-cycle modulation signal for tapering waveguide. These signals are fed to the laser pulse picker. Green dots show instant of pulses. 0 V and 2.5 V corresponds to closed and opened pulse picker, respectively. In lower graphs the modified RI area is shown in the material considering approximate spot size.

gradual change in the waveguide n_{eff} is a condition to minimize coupling power to high-order modes and/or radiation modes [19,20]. The profile of n_{eff} along propagation in the transition region can be easily programmed to be linear, exponential or any arbitrary functions [21].We demonstrate here a gradual transition by linearly increasing duty cycle that consequently will shrink the mode size to match the MFD of smf-28 optical fiber at 1550 nm (~10 μm).

Waveguide profiles are analyzed using a Photonova Ripper phase imaging system, which gives a tomographic projection image (x-y plane) of the cumulative phase transverse from the waveguide, that is in the z-axis of the sample [22].

3. Results and discussion

3.1. Positive index single track waveguide

Keldysh theory describes laser-matter interaction and can analyze phenomena like laser breakdown and high harmonic generation. Based on that theory tunneling ionization and multiphoton ionization are two limiting cases of the ionization induced by an electromagnetic field. The Keldysh parameter (γ) controls the regime of interaction. In the case of strong laser fields and low laser frequency that $\gamma << 1$ the tunneling ionization is dominant while at high laser frequencies (below resonance) and low intensities that $\gamma >> 1$ multiphoton ionization is dominant [23]. These

Optics EXPRESS

photoexcited electrons will now be the seed for the avalanche ionization process that eventually produces more electrons. By considering all of the contributed ionization mechanisms, the carrier generation rate describing evolution of electron density (N) as a function of laser intensity (I) can be written as [24]:

$$\frac{dN}{dt} = \alpha \mathrm{IN} + \mathrm{P(I)} \tag{2}$$

where α is the avalanche ionization coefficient and P is the nonlinear photoionization rate, that for $\gamma >> 1$ takes the form of:

$$P(I) = \sigma_m I^m \tag{3}$$

where σ_m is the multiphoton absorption coefficient and m is the number of photons required to cross the bandgap. In writing Eq. (2), the loss of electrons due to recombination and diffusion is ignored; since for pulses in the picosecond regime and shorter, it is negligible [25].

Avalanche ionization is dominant for a pulse longer than 100 fs [26], since it needs to accumulate a certain density of electron to exist. This non-linear trigger process followed by linear absorption gives us access to subwavelength writing resolution regime for a Gaussian intensity beam profile since the shoulder of the beam does not contribute if the intensity is not above threshold. This strategy was used in inscription of 1st order fiber Bragg grating into smf-28 fiber in [27] and they show that one can get higher RI modulation by reducing the pulse energy.

The final writing resolution voxel is not only determined by the focal spot size but by the entire energy process from photoionization to thermal stabilization. Therefore, heat and energy diffusion will influence the final RI affected area. Moreover, if the repetition rate of the laser is faster than the diffusion time, there will be thermal accumulation between pulses, assuming a spatial overlap. High temperature that can be achieved as a result of thermal accumulation [28] drastically increases the size of the modified area as shown on [5] for two different aluminosilicate-glasses. This inter-pulse accumulation regime will depend not only on the repetition rate but also on the pulse energy. In the meantime, the sign of the RI change seems to be dependent on the net fluence meaning that for lower net fluence, negative RI change (Fig. 2(a)) which will switch to positive for higher net fluences as reported in [5]. Similar RI changes were observed with low-iron soda lime glass, the difference between the two glasses is the fluence inversion threshold which is lower for our glass. Further increasing the net fluence leads to a nonuniform RI distribution, with a lower RI change in the center surrounded by higher positive side lobes. This limits the usable fluence range for waveguide inscription.

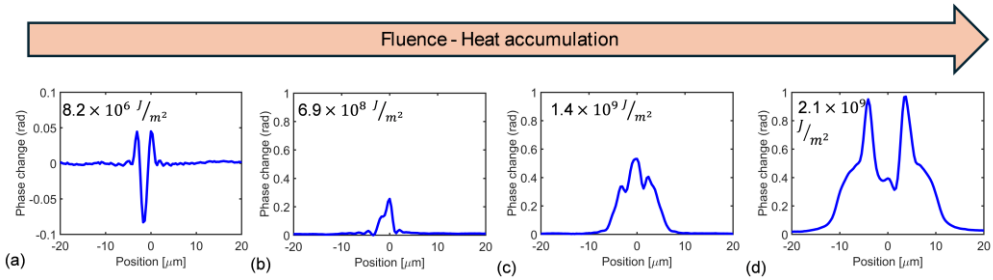

Fig. 2. (a-d) Phase change projection in the y-axis (integrated along the z-axis and averaged in the x-axis) for different fluence levels. Heat accumulation and thermal diffusion properties of material create bigger feature sizes at higher fluence. The writing parameters used are a scan speed of 50 mm/s, the repetition rate of 50.5 kHz and 300 mW optical power at (a) and 0.1 mm/s scan speed, the repetition rate of 606 kHz at (b-d). The power is changed from 50 mW to 150 mW in increment of 50 mW.

Optics EXPRESS

Therefore, the first step in writing the BGW was finding the exposure conditions leading to single-mode operation with the highest mode confinement as possible. However, a higher amount of fluence creates a higher RI change, because thermal accumulation also creates a bigger morphological change usually leading to multi-mode operation and reducing the RI contrast for the BG at first or second order, thus limiting the process to high-order gratings. Here in Fig. 2, the transverse phase change projections of the waveguide RI profile show the widening of the waveguide with increasing fluence. Adjusting fluence for one pass by varying the writing speed or repetition rate will increase heat accumulation and thus generate a more significant and spatially larger RI change. Further increase in heat accumulation (not shown in Fig. 2), could lead to a smaller index change, as the dip appearing in Fig. 2(d) becomes dominant. Although the induced RI change in (b-d) cases is positive, the lower fluence case in Fig. 2(b) yields a small enough feature to give a single-mode waveguide and first-order gratings. It is worth mentioning that the observed trend is not unique to the low-iron soda lime glass, as it is also observed with other types of compound glasses.

To systematically examine how various writing parameters affect the waveguiding properties of inscribed components, we applied the method described in [22] to reconstruct the RI profile using the phase projection of the RipperTM (Fig. 3). A geometrical model of RI profile was first built using a cross-section microscopy image of the waveguide (Fig. 3(b)). The features of the model were then adjusted using a genetic algorithm to fit the measured phase projection (Fig. 3(a)). The resulting RI profile of the BGW is shown in Fig. 3(c) and was used in finite element modeling (FEM) through COMSOL to recover the guided mode profile shown in Fig. 3(d). It is predicted that the phase profile shown in Fig. 3(a) leads to single-mode operation. Asymmetry in phase profile is likely an artifact of alignment or inhomogeneity in material.

The near-field modal profile of the inscribed BGW imaged with a 40× (0.55 NA) microscope objective onto a NanoScan beam profiler. Figure 3(e)-(g) presents this profile alongside the mode profile of an SMF-28 fiber for comparison. The MFD of BGW measured 19.5 μm and 21.2 μm along horizontal and vertical axes, respectively, showing ellipticity of 0.08.

3.2. Positive index single-pass BGW

The writing parameters (pulse energy, repetition rate, writing speed and pulse-picker modulation) are studied to generate a strong 35 dB BG reflection, low-loss and single-mode waveguide. The power and speed parameters are determined to optimize the waveguide RI profile, in a positive index regime, thus maximizing mode confinement while ensuring single-mode operation. The RI profile is considered as a DC index change, $\Delta n_{dc}(y, z)$, which is the average RI change over a grating period and is the transverse index profile viewed by the mode. In contrast, the longitudinal RI modulation amplitude $\Delta n_{ac}(x)$ will determines the grating reflectivity. While frequency of the keying function (on-off or FSK) is set by the writing speed (to match a Bragg period), the duty-cycle (for on-off) or frequency span (for FSK) is optimized to create the higher $\Delta n_{ac}(x)$. Since the MFD vs RI change profile $\Delta n_{dc}(y, z)$ determines the BG overlap, thus reflection strength, both optimizations are linked to one another. We find out that the BGWs written with the pulse energy of 165 nJ, the net fluence of $6.9 \times 10^8 \frac{J}{m^2}$, at the writing speed of 0.1 mm/s and the repetition rate of 303 kHz satisfy both above-mentioned conditions. We measured the peak DC RI change in the BGW to be 4.2×10^{-3} refractive index units (RIU). In the next step, the reconstructed RI profile is imported into COMSOL to compute the number of guided modes, MFD and mode overlap integral. The simulation results represent single-mode operation at 1550 nm with MFD 17.1 μm along the horizontal direction for either x- or y-polarized light in the waveguide, and 18.3 μm along vertical direction for either polarization which implies an overlap integral of 0.48 for the two orthogonal polarizations. Even though the modified RI cross-section is elliptical and is a combination of positive and negative parts, the propagation occurs inside the positive area. The presence of negative RI change, visible as a dark region in Fig. 3(b), suggests

Optics EXPRESS

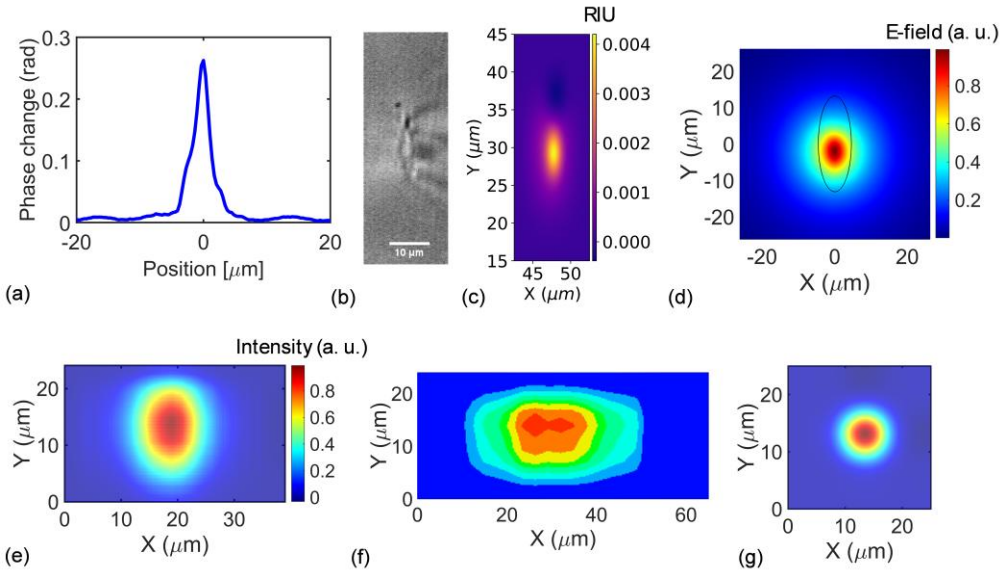

Fig. 3. (a) Measured phase profile of 1st order BGW written based on on-off keying at duty cycle of 50%. (b) The cross-section image of BGW. (c) The reconstructed RI profile of BGW peaks at value of 4.2 $\times 10^{-3}$ refractive index unit (RIU) and (d) Simulated electric field form the y-polarized mode. The simulation result predicts single-mode operation. The black ellipse represents the approximate size of the modified area obtained from the reconstructed RI profile which is about 9 μm × 26 μm. (e) The near-field mode profile of fs-inscribed BGW at 1550 nm, (f) at Bragg resonance wavelength and (g) smf-28 fiber at 1550 nm imaged with 40X objective on NanoScan beam profiler. Figure 3(e)-(g) share the same colour bar.

the possible formation of nanograting or nanoporous structures [29–31]. The negative part makes the mode more confined which helps generate a more symmetrical mode profile (Fig. 3(d)-(e)) without compromising guidance properties of inscribed waveguides. The birefringence (Δn) of a simulated BGW is about 4.07 $\times 10^{-7}$.

The spectral response of written first-order BGWs is measured by a Luna OBR 4600 optical frequency domain reflectometry (OFDR) system with a polarization controller. The effect of the waveform duty cycle is found to be significant on the grating response. Deviation from sinusoidal modification decreases the Fourier component of the modulated RI at the Bragg wavelength. Also, the spectral red shift occurs with an increase in duty cycle, which implies an increasing BGW n_{eff}. This is an important fact that must be considered in designing apodized gratings. By comparing 1st to 3rd orders gratings with on-off keying and FSK modulations, the best performance, shown in Fig. 4, was achieved using 1st order BGs with on-off keying at a 50% duty cycle.

Another factor influencing grating strength is the fs laser's polarization state relative to the scan direction. The polarization of fs laser is linear, and it is rotated using a half-wave plate. As shown in Fig. 4(b), whenever the scan direction is parallel to the light polarization, the BGW is stronger (10 dB difference in transmission) and exhibits less parasitic side-modes. The dependency of grating strength on polarization of the writing laser likely arises from the formation of nanogratings [32,33] that are observed in pristine fused silica [34], Ge-doped silica glasses [35] and compound glasses [36]. These periodic nanostructures exhibit interesting properties; one of them is anisotropic light scattering which peaks in the plane of light polarization, interpreted by the movement of photoelectrons along the direction of light polarization that induces RI

Optics EXPRESS

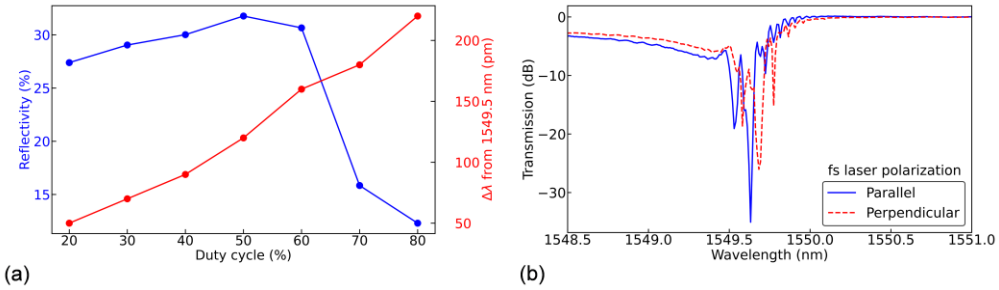

Fig. 4. (a) Effect of pulse-picker on-off keying duty cycle on BG reflectivity (left axis) and center Bragg wavelength (shown around 1549.5 nm) (right axis). (b) Example of strong BG for net fluence of 6.9 $\times 10^8$ $\frac{\text{J}}{\text{m}^2}$ written with different fs laser linear polarization. Parallel pol. (blue line) is oriented in writing direction (along the x-axis), while in the perpendicular case, the fs laser polarization is oriented along the y-axis.

inhomogeneities [35]. Parallel exposure (Fig. 4(b), blue curve) shows a strong secondary dip at lower λ which is believed to be cross-coupling (from fundamental mode) to an unexpected high-order lossy modes (LP_{11}-like) in our waveguide. While the V-number is below the multimode cutoff, it is very close. Therefore, local RI fluctuations and fabrication imperfections such as an unwanted tilt angle in the RI profile can excite leaky higher-order mode. Suppressing this leaky mode remains under investigation. The presence of LP_{11}-like mode was confirmed by viewing the near-field output mode at the transmission loss dips (attenuating the fundamental mode) which did show in Fig. 3(f) the presence of a higher order mode. Perpendicular exposure yields more dips that are highly polarization dependent, indicating that the resulting RI profile is not only different from our previously modeled profile in Fig. 3, but also highly anisotropic, likely from the presence of nanograting or nanoporous structures. Both cases show strong radiation loss at lower wavelength, resulting in a 3.4 dB loss. This mostly arises from asymmetry in the profile of induced RI change that is associated with 1° tilt angle. Circular polarization is to address the issue related to nanograting formation, potentially reducing propagation and radiation losses [37,38]. However, this feature was not available in our setup. Consequently, we conducted our investigations solely with linear polarizations. Since parallel exposure leads to higher quality BG, all further study used such a fs laser polarization. The best BGW has shown propagation loss of 0.94 dB/cm.

3.3. Single-mode tapered waveguide for low-loss coupling to single-mode fiber

In Fig. 5(a)-(b) the phase change and reconstructed RI profile of a waveguide written with the pulse energy of 165 nJ, the net fluence of 3.4 $\times 10^8$ $\frac{\text{J}}{\text{m}^2}$ at the writing speed of 0.2 mm/s and the repetition rate of 303 kHz, are shown. For the waveguide shown in Fig. 5(a)-(b) the waveform duty cycle was adjusted to 50% yielding a period of 100 nm short enough to ensure pulse to pulse overlap but no Bragg matching condition in the C-band. To match the mode profile of the written waveguide with SMF-28, the waveguide was tapered (reducing MFD gradually) by linearly increasing the duty cycle from 50% to 100% along 15 mm by increasing pulse number at the rate of 5.05 $\times 10^4$ pulses/mm from 7.575 $\times 10^5$ to 1.515 $\times 10^6$. The phase change and reconstructed RI profiles of the tapered waveguide associated with 100% duty cycle at the end of the facet are demonstrated in Fig. 5(c)-(d), respectively. The COMSOL simulation results predict single-mode operation at a wavelength of 1550 nm for waveguides written at duty cycles of 50% and 100%. For un-tapered waveguide, the MFD of the guided mode is calculated to be 25.32 μm (24.96 μm) along horizontal direction for x (y) polarized light, and 30.89 μm (30.41 μm) along vertical direction for x (y) polarized light. At the end of the taper, the MFD of the fundamental

Optics EXPRESS

mode is 11.58 μm (11.70 μm) along horizontal direction for x (y) polarized light, and 13.57 μm (13.57 μm) along vertical direction for x (y) polarized light. To confirm the consistency of our simulation results, MFDs of un-tapered waveguide (Fig. 5(a)-(b)) and tapered waveguide (Fig. 5(c)-(d)) are measured.

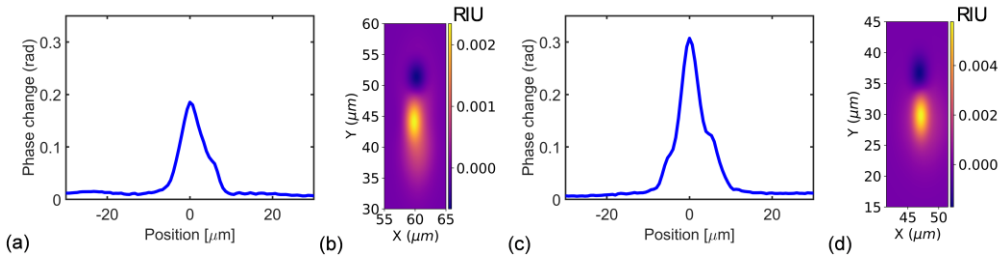

Fig. 5. (a) Measured phase profile of an un-tapered waveguide inscribed at a 50% duty cycle. (b) The reconstructed RI profile of a waveguide with phase profile showing in Fig. 5(a) peaks at the value of 2.3 $\times 10^{-3}$ RIU. (c) Measured phase profile of a tapered waveguide inscribed at a 100% duty cycle. (d) The reconstructed RI profile of a waveguide with phase profile showing in Fig. 5(c) peaks at the value of 5.8 $\times 10^{-3}$ RIU.

The near-field modal profiles at the output of the waveguides are measured with an end-fire coupling system at 1550 nm. The input beam was butt-coupled at the input face of the sample, and the output near-field modal profiles were recorded by imaging the waveguides with a 40× (0.55 NA) microscope objective onto a NanoScan beam profiler. MFD measurement of un-tapered waveguide showing a reduction in mode size up to 46.9% by tapering, which can significantly improve coupling efficiency (η) to the SMF-28 fiber. To estimate the magnitude of η, we use the simulation results to calculate it according to [14]:

$$\eta = \frac{|\int E_1^* E_2 dA|^2}{\int |E_1|^2 dA \int |E_2|^2 dA} \tag{4}$$

where E_1 and E_2 are electric field amplitude of fiber and inscribed waveguide, respectively. The A represents the integration area around the mode profile. Simulation shows an increase in η from 29% to 68%. Results of MFD measurements for vertical and horizontal axes are shown separately in Table 1. Measurement results are in good agreement with MFDs calculated from simulation.

Table 1. Comparison between the measured mode size of tapered and un-tapered waveguides at 1550 nm. V and H denote vertical and horizontal axes, respectively.

	Un-tapered waveguide MFD (μm)	Tapered waveguide MFD (μm)	Relative change of MFD
V axis	23.8 ± 0.8	13.1 ± 0.1	45.0%
H axis	22.9 ± 0.2	12.1 ± 0.03	46.9%

Tapering down of MFD enhances coupling into the optical fiber by an amount of 3.26 dB. The measured coupling efficiency is calculated by measuring total losses and removing the waveguide propagation losses of 1.26 ± 0.1 dB. However, simulations predict a slightly higher improvement of 3.7 dB. The coupling efficiency potentially can be increased further by designing a transition region in order to satisfy an adiabatic condition, which was not studied in this article.

3.4. *No-bend* 2 × 2 *symmetric coupler*

The versatility of this single-pass writing technique is further demonstrated by applying the taper method of section 3.3 to a functional device, that is a 2 × 2 coupler. Another advantage

Optics EXPRESS

of this technique is that the coupler can be designed without any bends involved, augmenting miniaturisation potential and avoiding bend losses, thereby offering an effective solution to the loss limitations typically encountered in designing photonics circuits with low-NA waveguides, commonly the case in fs laser written components.

As shown in section 3.3, the MFD is proportional to the number of pulses. Gradual change in waveform duty cycle results in pulse number change and consequently MFD alters gradually. Hence for inscribing no-bend coupler, we started first by a waveform with 100% duty cycle which guarantees more localized mode near the input ports. Then duty cycle decreases linearly along 15 mm length of waveguide from 100% to 50%. At this position the MFD which is now almost doubled is large enough to beat with the waveguide in its vicinity. The waveform duty cycle is kept at 50% in the coupling region to inscribe the waveguide with a length equal to 23.2 mm. Long enough to ensure power transfer between two waveguides will take place. Afterwards, the waveform duty cycle increases from 50% to 100% along 15 mm to decrease coupling losses to fiber in the output facet.

Since the coupler is symmetric, the second waveguide is written with the same waveform but at a certain distance from the first waveguide. The schematic of symmetric no-bend 2 $\times$ 2 coupler is shown in Fig. 6(a). The gradual colour change corresponds to gradual change in RI.

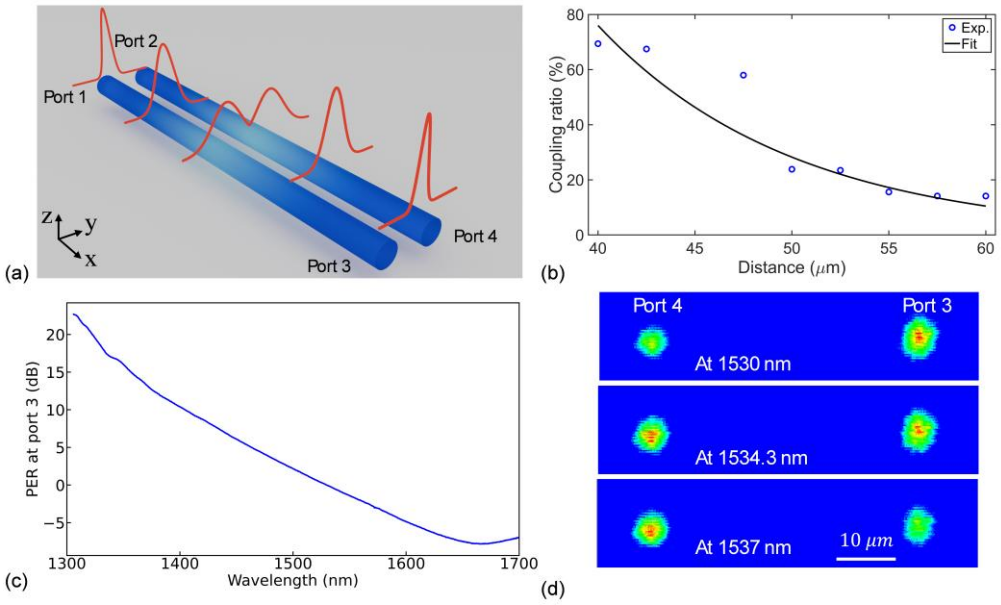

Fig. 6. (a) Schematic of symmetric no-bend 2 $\times$ 2 coupler. Gradual change in RI is shown by gradual colour change from high RI (dark blue) to low RI (light blue). We assumed that coupler length is equal L_π that complete energy transfer takes place. (b) Dependence of Port 4's coupling ratio at 1550 nm on the separation distance between two waveguides. Blue circles represent measured data, while the black line shows the exponential fit to the experimental results. (c) Wavelength dependency of PER at the port 3 of the coupler with a separation distance of 47.5 μm, and a coupling length of 23.2 mm. (d) The near-field mode profile of the same coupler for output ports is shown at three different wavelengths. The two waveguides are written at the speed of 0.2 mm/s, the repetition rate of 303 kHz, with the pulse energy of 165 nJ and the net fluence of 3.4 $\times 10^8 \frac{\text{J}}{\text{m}^2}$.

Optics EXPRESS

By assuming that port 1 is the excitation port that light is launched through, the coupling ratio between two ports of the coupler, r, is defined as [39]:

$$r = \frac{P_4}{P_3 + P_4} = \frac{\kappa^2}{\delta^2} sin^2(\delta L) \tag{5}$$

where $\delta = \sqrt{\frac{(\beta_1 - \beta_2)^2}{4} + \kappa^2}$, and β_1, β_2, κ and L are propagation constants of two waveguides, coupling constant and coupler length, respectively. In the strong coupling regime that two adjacent waveguides are usually close, the material modification during the first waveguide inscription will change the RI profile of the second waveguide, therefore $\beta_1 \neq \beta_2$ and the coupling ratio will be lower than 100%. We decided to inscribe waveguides in lateral distances varying from 40 μm to 60 μm, large enough to be in a weak coupling regime and prevent RI modification by previous exposure.

As discussed in [40], the κ decreases exponentially by increasing the waveguides' separation. Hence, in the weak coupling regime, the coupling ratio also decreases exponentially by separation increase as can be seen in Fig. 6(b). The exponential function is fitted on experimental results at the wavelength of 1550 nm.

For center-to-center distance of 47.5 μm, the power extinction ratio (PER) at port 3 as a function of wavelength is shown in Fig. 6(c), there is 3 dB coupling between two waveguides at 1534.3 nm which can be seen also from the near-field mode pattern imaged by phosphor-coated CCD camera (Fig. 6(d)). The coupler has a coupling constant of 37.3 m^{-1} which can be increased by reducing separation distance or enhancing MFD in the interaction region. Since the bending loss is eliminated in this method, the waveform duty cycle can be decreased further in the coupling area without incorporating additional loss while increasing κ.

4. Conclusion

The capability of controlling the number of fs laser pulses allowed the fabrication of BGWs, tapered waveguides and couplers in a single writing step with positive index change in low-iron soda lime glass. A positive index waveguide with relatively strong mode confinement is written inside a low-iron soda lime glass sample using the fs laser. It was found that the pulse energy of 165 nJ and the net fluence of $3.4 \times 10^8 \frac{J}{m^2}$ result in an RI change of 5.8×10^{-3}. A strong mode confinement with an MFD of 13.1 μm and 12.1 μm along vertical and horizontal axes, respectively, was observed. Simulation yields single-mode operation. Strong 1st order grating with a transmission dip of 35 dB corresponding to a reflectivity of 99.96%, propagation loss of 0.94 dB/cm and radiation loss of 3.4 dB, were demonstrated. The inscribed tapered waveguide resulted in a relative change of MFD of more than 45.0%. Tapering down MFD facilitates the coupling of light from inscribed elements into the SMF-28 optical fiber which reduced coupling loss by amount of 3.26 dB. No-bend couplers with coupling constants ranging from 16.6 m^{-1} to 42.4 m^{-1} were inscribed thanks to the precise control of MFD, effectively eliminating bending loss along propagation. The simplicity of waveform programming and its robustness by avoiding nonlinear peak-power dependence offers an effective approach for designing asymmetrical couplers made of low NA waveguides, a common characteristic of fs-inscribed waveguides. Our results demonstrate that high-functional optical elements can be fabricated in an inexpensive low-iron soda lime glass, and creates an opportunity for mass production of photonic circuits at a lower cost than fused silica, with potential applications in microfluidics and integrating optical circuits inside solar panels.

Funding. Natural Sciences and Engineering Research Council of Canada (NSERC-ALLRP 580549 - 22).

Acknowledgment. The authors thank Qingtao Chen for assistance with waveguide characterization.

Disclosures. The authors declare no conflicts of interest.

Optics EXPRESS

Data availability. Data underlying the findings presented in this paper are not publicly available at this time but may be obtained from the authors upon reasonable request.

References

1. R. R. Gattass and E. Mazur, "Femtosecond laser micromachining in transparent materials," Nat. Photonics **2**(4), 219–225 (2008).
2. G. R. Castillo, L. Labrador-Paez, F. Chen, *et al.*, "Depressed-Cladding 3-D Waveguide Arrays Fabricated With Femtosecond Laser Pulses," J. Lightwave Technol. **35**(13), 2520–2525 (2017).
3. Q. Chen, J.-S. Boisvert, M. S. Sharawi, *et al.*, "Bragg gratings with novel waveguide models fabricated in bulk glass via fs-laser writing and their slow-light effects," Opt. Express **32**(1), 188–204 (2024).
4. K. Miura, J. Qiu, H. Inouye, *et al.*, "Photowritten optical waveguides in various glasses with ultrashort pulse laser," Appl. Phys. Lett. **71**(23), 3329–3331 (1997).
5. J.-S. Boisvert, S. Loranger, and R. Kashyap, "Fs laser written volume Raman–Nath grating for integrated spectrometer on smartphone," Sci. Rep. **13**(1), 13717 (2023).
6. G. D. Marshall, M. Ams, and M. J. Withford, "Direct laser written waveguide-Bragg gratings in bulk fused silica," Opt. Lett. **31**(18), 2690–2691 (2006).
7. H. Zhang, S. M. Eaton, and P. R. Herman, "Single-step writing of Bragg grating waveguides in fused silica with an externally modulated femtosecond fiber laser," Opt. Lett. **32**(17), 2559–2561 (2007).
8. H. Zhang, S. M. Eaton, J. Li, *et al.*, "Type II high-strength Bragg grating waveguides photowritten with ultrashort laser pulses," Opt. Express **15**(7), 4182–4191 (2007).
9. J. R. Grenier, L. A. Fernandes, J. S. Aitchison, *et al.*, "Femtosecond laser fabrication of phase-shifted Bragg grating waveguides in fused silica," Opt. Lett. **37**(12), 2289–2291 (2012).
10. P. Zeil, C. Voigtländer, J. Thomas, *et al.*, "Femtosecond laser-induced apodized Bragg grating waveguides," Opt. Lett. **38**(13), 2354–2356 (2013).
11. S. Gross, M. Dubov, and M. J. Withford, "On the use of the Type I and II scheme for classifying ultrafast laser direct-write photonics," Opt. Express **23**(6), 7767–7770 (2015).
12. J. Cardenas, C. B. Poitras, K. Luke, *et al.*, "High Coupling Efficiency Etched Facet Tapers in Silicon Waveguides," IEEE Photonics Technol. Lett. **26**(23), 2380–2382 (2014).
13. S. Gross, N. Riesen, J. D. Love, *et al.*, "Three-dimensional ultra-broadband integrated tapered mode multiplexers," Laser Photonics Rev. **8**(5), L81–L85 (2014).
14. R. Heilmann, C. Greganti, M. Gräfe, *et al.*, "Tapering of femtosecond laser-written waveguides," Appl. Opt. **57**(3), 377–381 (2018).
15. L. Ramousse, G. Chériaux, C. Claudet, *et al.*, "Femtosecond laser-induced damage threshold of nematic liquid crystals at 1030 nm," Appl. Opt. **60**(26), 8050–8056 (2021).
16. V. R. Bhardwaj, E. Simova, P. B. Corkum, *et al.*, "Femtosecond laser-induced refractive index modification in multicomponent glasses," J. Appl. Phys. **97**(8), 083102 (2005).
17. J.-P. Bérubé, M. Bernier, and R. Vallée, "Femtosecond laser-induced refractive index modifications in fluoride glass," Opt. Mater. Express **3**(5), 598–611 (2013).
18. T. Erdogan, "Fiber grating spectra," J. Lightwave Technol. **15**(8), 1277–1294 (1997).
19. T. A. Birks and Y. W. Li, "The shape of fiber tapers," J. Lightwave Technol. **10**(4), 432–438 (1992).
20. F. Jafari, O. R. Ranjbar-Naeini, M. I. Zibaii, *et al.*, "Profilometry of an optical microfiber based on modal evolution," Opt. Lett. **45**(24), 6607–6610 (2020).
21. A. Horth, P. Cheben, J. H. Schmid, *et al.*, "Ideal, constant-loss nanophotonic mode converter using a Lagrangian approach," Opt. Express **24**(6), 6680–6688 (2016).
22. A. Drouin, P. Lorre, J.-S. Boisvert, *et al.*, "Spatially resolved cross-sectional refractive index profile of fs laser-written waveguides using a genetic algorithm," Opt. Express **27**(3), 2488–2498 (2019).
23. L. V. Keldysh, "Ionization in the field of a strong electromagnetic wave," Sov. Phys. JETP **20**(5), 1307–1314 (1965).
24. C. B. Schaffer, A. Brodeur, and E. Mazur, "Laser-induced breakdown and damage in bulk transparent materials induced by tightly focused femtosecond laser pulses," Meas. Sci. Technol. **12**(11), 1784–1794 (2001).
25. D. Du, X. Liu, G. Korn, *et al.*, "Laser-induced breakdown by impact ionization in SiO2 with pulse widths from 7 ns to 150 fs," Appl. Phys. Lett. **64**(23), 3071–3073 (1994).
26. P. P. Rajeev, M. Gertsvolf, P. B. Corkum, *et al.*, "Field Dependent Avalanche Ionization Rates in Dielectrics," Phys. Rev. Lett. **102**(8), 083001 (2009).
27. A. Roberge, S. Loranger, J.-S. Boisvert, *et al.*, "Femtosecond laser direct-writing of high quality first-order Bragg gratings with arbitrary complex apodization by phase modulation," Opt. Express **30**(17), 30405–30419 (2022).
28. S. M. Eaton, H. Zhang, P. R. Herman, *et al.*, "Heat accumulation effects in femtosecond laser-written waveguides with variable repetition rate," Opt. Express **13**(12), 4708–4716 (2005).
29. E. Bricchi, B. G. Klappauf, and P. G. Kazansky, "Form birefringence and negative index change created by femtosecond direct writing in transparent materials," Opt. Lett. **29**(1), 119–121 (2004).
30. J. Canning, M. Lancry, K. Cook, *et al.*, "Anatomy of a femtosecond laser processed silica waveguide [Invited]," Opt. Mater. Express **1**(5), 998–1008 (2011).
31. M. Sakakura, Y. Lei, L. Wang, *et al.*, "Ultralow-loss geometric phase and polarization shaping by ultrafast laser writing in silica glass," Light: Sci. Appl. **9**(1), 15 (2020).

Optics EXPRESS

32. Y. Lei, H. Wang, L. Skuja, *et al.*, "Ultrafast Laser Writing in Different Types of Silica Glass," Laser Photonics Rev. **17**(7), 2200978 (2023).
33. Y. Shimotsuma, P. G. Kazansky, J. Qiu, *et al.*, "Self-Organized Nanogratings in Glass Irradiated by Ultrashort Light Pulses," Phys. Rev. Lett. **91**(24), 247405 (2003).
34. V. R. Bhardwaj, E. Simova, P. P. Rajeev, *et al.*, "Optically Produced Arrays of Planar Nanostructures inside Fused Silica," Phys. Rev. Lett. **96**(5), 057404 (2006).
35. P. G. Kazansky, H. Inouye, T. Mitsuyu, *et al.*, "Anomalous Anisotropic Light Scattering in Ge-Doped Silica Glass," Phys. Rev. Lett. **82**(10), 2199–2202 (1999).
36. S. S. Fedotov, R. Drevinskas, S. V. Lotarev, *et al.*, "Direct writing of birefringent elements by ultrafast laser nanostructuring in multicomponent glass," Appl. Phys. Lett. **108**(7), 071905 (2016).
37. M. Ams, G. D. Marshall, and M. J. Withford, "Study of the influence of femtosecond laser polarisation on direct writing of waveguides," Opt. Express **14**(26), 13158–13163 (2006).
38. Y. Lei, G. Shayeganrad, H. Wang, *et al.*, "Efficient ultrafast laser writing with elliptical polarization," Light: Sci. Appl. **12**(1), 74 (2023).
39. S. M. Eaton, W. Chen, L. Zhang, *et al.*, "Telecom-Band Directional Coupler Written With Femtosecond Fiber Laser," IEEE Photonics Technol. Lett. **18**(20), 2174–2176 (2006).
40. A. W. Snyder and J. D. Love, "MODES OF TWO PARALLEL FIBERS," in *Optical waveguide theory* (Springer, 1983), pp. 392.